IEEE Access
Multidisciplinary ⋮ Rapid Review ⋮ Open Access Journal

Received October 20, 2021, accepted November 3, 2021, date of publication November 8, 2021, date of current version November 15, 2021.

Digital Object Identifier 10.1109/ACCESS.2021.3126640

Low Mutual Coupling Design for 5G MIMO Antennas Using Multi-Feed Technology and Its Application on Metal-Rimmed Mobile Phones

ZHONGWEI JI[1], YUKE GUO[2], YUQI HE[2], LUYU ZHAO[2], (Senior Member, IEEE), GUAN-LONG HUANG[3], (Senior Member, IEEE), CHUANGZHU ZHOU[1], QINJUAN ZHANG[4], AND WEI LIN[5], (Senior Member, IEEE)

[1]ZTE Communications Company Ltd., Shenzhen, Guangdong 518057, China
[2]Key Laboratory of Antennas and Microwave Technologies, Xidian University, Xi'an 710071, China
[3]School of AI-Guangdong and Taiwan, Foshan University, Foshan, Guangdong 528225, China
[4]China Academy of Information and Communications Technology, Beijing 100191, China
[5]Global Big Data Technologies Centre, University of Technology Sydney, Ultimo, NSW 2007, Australia

Corresponding author: Luyu Zhao (lyzhao@xidian.edu.cn)

This work was supported by the National Key Research and Development Program of China under Grant 2019YFF0216600.

ABSTRACT In this paper, an effective method for developing a multi-feed multiple-input multiple-output (MIMO) antenna system using the metal rims of a mobile phone without any structural interruption on the long edge frames is proposed. Instead of traditionally designing MIMO antennas with multiple similar antenna structures on the mobile phone frame or its ground plane, the MIMO antennas in this work are realized by reasonably constructing feeding points and grounding points on the entire edge frame. The MIMO antenna system established by such multi-feed technique is capable to achieve much simpler structural configuration, excellent isolation and matching performance while multiple antennas are connected. A planar eight-port MIMO antenna system operating in the 5G frequency band of 3.4∼3.6 GHz is investigated initially, and subsequently applied to the curved metal-rims which comply with the industry design of a modern flagship mobile phone. The prototypes are fabricated and measured, evaluation results show that isolations among all ports are better than 15 dB with reflection coefficients below −10 dB within the band of 3.4∼3.7 GHz and −6 dB within the band of 3.3∼3.8 GHz. In addition, more than 57% total efficiency and envelope correlation coefficient (ECC) of less than 0.3 are obtained. The satisfactory performance reveals the proposed design of multi-feed MIMO antennas can be a promising candidate for 5G metal-rimmed mobile phone applications.

INDEX TERMS 5G mobile communication, antenna decoupling, mobile phone antenna, multiple-input multiple-output (MIMO), multi-feed technology, mutual coupling.

I. INTRODUCTION

As the public demand on higher data rate and throughput increases rapidly in recent years, the development of communication theories and technologies has to be greatly advanced. Though the current fourth-generation (4G) long term evolution (LTE) mobile communication system has been widely deployed, it is quite difficult to further provide consumers with experience of much higher data rate and lower latency within the current protocols. Therefore, it is imperative to increase the operating bandwidth or utilize the spatial diversity so as to greatly enhance the system's channel capacity and spectrum efficiency. Since the low-frequency spectrum resources are very limited and expensive, it is unrealistic to directly expand the antenna's operating bandwidth for larger channel capacity. Although it is possible to reform 4G spectrum while deploying 5G communication systems, it is still under discussion and development [1]. Another way is to enhance the application and performance of multiple-input multiple-output (MIMO) antenna systems, which are able to introduce more communication paths to boost the data rate. Hence, MIMO antenna architecture is believed to

The associate editor coordinating the review of this manuscript and approving it for publication was Stefan Schwarz.

be wildly applied in mobile terminals for the 5G wireless communication system without extra frequency resources.

Furthermore, it is well-known that the clearance area for mobile phone antennas is getting very stringent, which in turn squeezes the space for MIMO antenna system deployment. When multiple antennas of the MIMO system are placed closely to each other in smartphones, the co-existence or the mutual coupling problem of the MIMO antennas would become very serious [2], [3]. There are many decoupling approaches reported in literatures and the majority of them introduce additional structures like artificial structures and neutralization-lines to achieve isolation improvement [4]–[8]. Using decoupling networks made of lumped elements or coupled resonators are also reported in [4], [9]–[13]. A recent progress on MIMO antenna decoupling by using characteristic mode without adding any extra structures or circuits have been reported [14], [15]. Good isolation is achieved by fixing an antenna while placing other antennas at the stable null-points of the electric-fields excited by the fixed antenna [15]. From another perspective, applying diversity techniques on antenna polarization and pattern can also achieve high isolation and low envelope correlation coefficient (ECC) among multi-element antennas, but it has to occupy a sufficient space in the mobile terminals to realize such techniques [16], [17], [19], which is infeasible for future 5G phones integrated with more and more functional electronic components to realize more fantabulous performances. Recently, spatial reuse method has been widely used in designing at least 8 MIMO antennas in a mobile terminal. Orthogonal radiation modes is obtained by properly designing the antennas within an antenna unit made of two antennas, and has achieved very good results [26]–[31]. However, there are no further measures taken to improve the isolation between the antenna units, in most cases, they are naturally placed and separated. Therefore, regarding practical applications, the above-mentioned decoupling approaches and the MIMO antennas placement strategies are difficult to implement to full-screen mobile terminals surrounded by metal frames/rims as signals would be blocked by the rims. A traditional solution to alleviate such problem is to destroy the structural integrity and cut slots on the metal rims of the phones so as to achieve good electromagnetic (EM) wave radiation and proper antenna operation frequency. Thus, it forms the motivation of this paper to explore an efficient design methodology to realize the MIMO antenna system by directly exciting the metal rims of the mobile phone without adding additional structures, components or breaking the integrity of the metal rims on both long edge of a mobile terminal.

This work proposes an 8-element MIMO antenna system with good isolation and radiation for 5G smartphone applications. Compared with existing decoupling methods, it possesses the following unique features:

1) The structural configuration of the proposed MIMO antenna is simple and easy for practical mobile phone implementation. The 8-element MIMO antenna system is formed by directly exciting the side metal rims based on the multi-feed technology [20]. No additional antenna structures or circuits are required.

2) The radiation patterns of the proposed MIMO antenna element have a wide coverage range. Since there are two groups of orthogonal radiation patterns within the 8-element antennas which are complementary to each other, the proposed antenna system is robust with respect to different usage scenarios and holding positions of the mobile phone.

3) The proposed antenna system is only designed on the two sides of the mobile metal rims without destroying their integrity. It not only well maintains the robustness of the mobile phone, but also is space-saving.

The remaining part of this paper is organized as follows. Section II introduces the antenna evolution process and theoretical analysis of the proposed multi-feed MIMO antenna system realized in a planar style. An 8-port MIMO antenna system designed in practical curved metal-rims of mobile phone associated with experimental results is illustrated in detail in Section III. Section IV draws the conclusions of the whole paper.

II. DESIGN EVOLUTION OF MIMO ANTENNAS IN PLANAR STRUCTURE

In this section, the design evolution process of the proposed planar MIMO antennas from a dual-feed element (Antenna A) to an eight-feed antenna system (Antenna D) is illustrated in Fig. 1. Antenna A is the basic dual-feed antenna module which acts as the building block for the final multi-feed antenna system. Antenna B is a quad-feed antenna subsystem without any breaking points, formed by two dual-feed antenna modules. An eight-feed MIMO antenna system (Antenna C) can be considered as formed by two Antenna Bs arranged at two sides of the mobile phone. Additionally, four grooves are etched on the ground plane of the final planar MIMO antenna system in order to further reduce the mutual coupling between the metallic radiators on both sides, as shown in the configuration of Antenna D in Fig.1. The design details and antenna performances will be discussed as follows.

A. DESIGN OF THE DUAL-FEED ANTENNA MODULE

A detail view of the dual-feed antenna module (Antenna A) is shown in Fig. 2, which can be considered as an evolution from the combination of two types of radiators: a planar inverted-F antenna (PIFA) and a loop antenna [21], [22]. The antenna module is designed on a 90 mm $\times$ 50 mm printed circuit board (PCB) with low-cost FR-4 substrate, the substrate thickness, copper layer thickness, dielectric constant and loss tangent of which are 0.8 mm, 0.035 mm, 4.4 and 0.02, respectively. The printed copper line marked with orange color is the main radiator with four branches from the top view, two of which are shorted branches with length and width of 7 mm and 1.5 mm respectively, and the other two are feeding branches with 8.5 mm long and 1.5 mm width. The two antennas share the shorted branch between Port 1 and

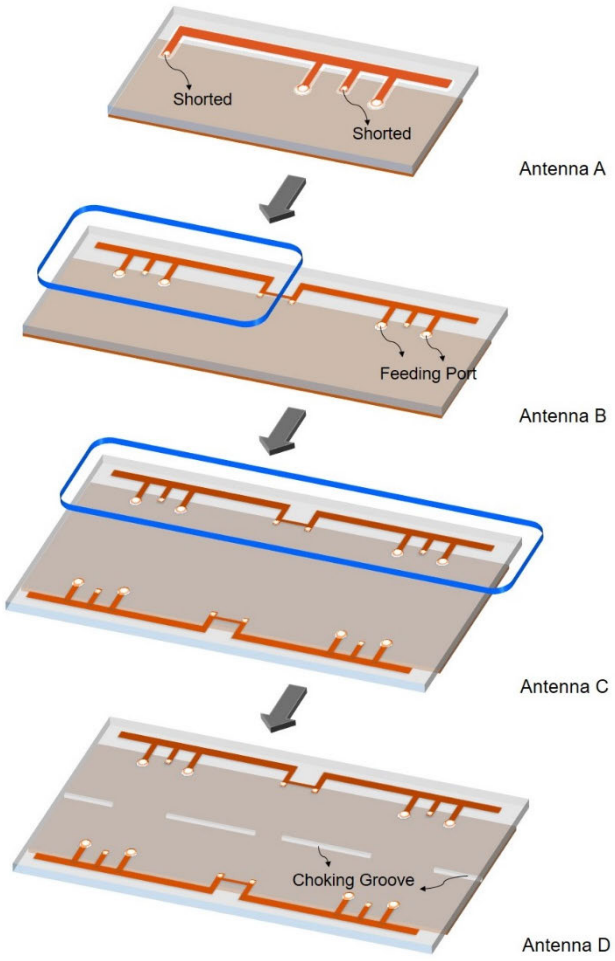

FIGURE 1. Evolution process of the proposed planar multi-feed MIMO antenna system: Antenna A, Antenna B and Antenna C are the dual-feed, quad-feed and eight-feed MIMO antennas; Antenna D is the eight-feed MIMO antenna with decoupling design.

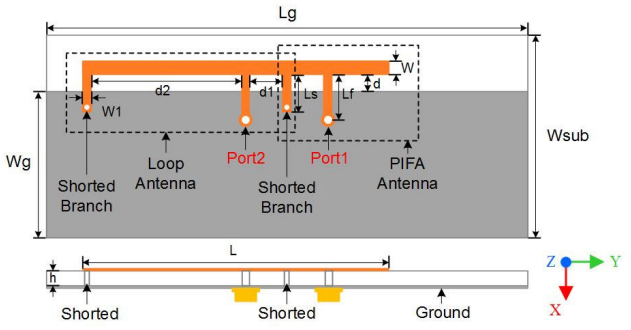

FIGURE 2. Structural diagram of the dual-feed MIMO antenna module.

Port 2. In addition, the common ground plane of the PIFA radiator and the loop radiator is printed on the bottom-side of the substrate, as the grey color portion marked in Fig. 2. The detail dimensions of the dual-feed antenna module are already given in Table 1.

In order to achieve good decoupling performance, the spacing between the two feeding ports and the shorted branch in the middle should satisfy equation (1) as it is known that the current distribution on the radiator would reach its minimum after travelling a quarter wavelength

TABLE 1. Detail dimensions of the dual-feed MIMO antenna shown in Fig. 2 (unit: mm).

Parameters	Values	Parameters	Values
W_g	39	d_1	6.5
L_g	90	d_2	28
W_{sub}	50	L_s	7
W	2.5	L_f	8.5
W_1	1.5	L	57
d	3.5	h	0.8

$$L_f + d_1 + L_s \approx 0.25\lambda \tag{1}$$

In equation (1), the lengths of L_f, d_1 and L_s are around 0.1 λ, 0.08 λ and 0.08 λ, respectively (λ is the wavelength of the center operating frequency 3.5 GHz in free-space). In order to further understand the working and decoupling mechanism, the dual-feed antenna module is separated into two independent antennas along the shorted branch between the two feeding ports for better illustration, as shown in Fig. 3. The separated model can be considered as counterpart antennas to the proposed antenna module shown in Fig. 2, the corresponding dimensions of which are exactly the same as the proposed dual-feed antenna. From the numerical results in Fig. 4, the simulated reflection coefficient of the proposed antenna and the counterpart antennas are close to each other, which proves that the proposed dual-feed antenna is basically made up of the two independently-working antennas but merged into one antenna by sharing the common shorted branch and almost no effect is introduced into their resonance thanks to the spacing relationship shown in equation (1). Fig. 5 shows the simulated S-parameter of the proposed dual-feed MIMO antenna module.

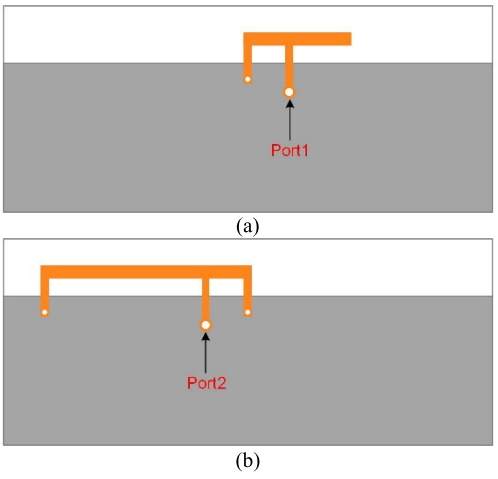

FIGURE 3. Geometry of the counterpart antennas. (a) PIFA antenna. (b) Loop antenna.

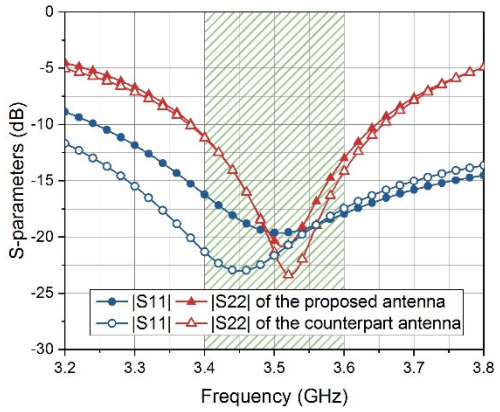

FIGURE 4. Simulated reflection coefficients of the proposed antenna and the counterpart antennas: S11 and S22 of the proposed antenna represent the reflection coefficients of the Port 1 and Port 2 of the dual-feed antenna respectively; S11 and S22 of the counterpart antennas represent the reflection coefficients of the PIFA antenna (excited at Port 1 in Fig. 3) and the loop antenna (excited at Port 2 in Fig. 3) respectively.

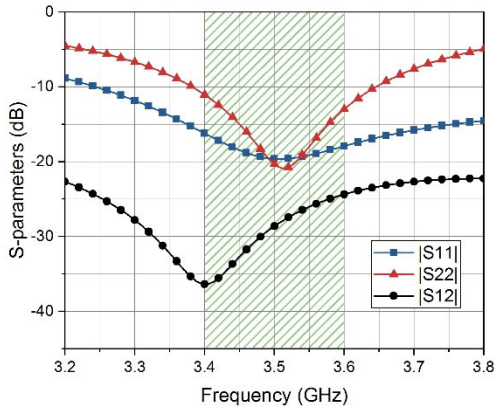

FIGURE 5. Simulated S-parameter of the dual-feed MIMO antenna module.

The operating frequency band of the PIFA antenna (Port 1 excited) is 3.25∼3.8 GHz (15.6% relative bandwidth) and the loop antenna (Port 2 excited) is 3.38∼3.64 GHz (7.4% relative bandwidth) with reflection coefficient less than −10 dB. Both of the bandwidths with reflection coefficient less than −6 dB are able to cover the frequency band of interest (3.4∼3.6 GHz, 5G NR band N78) for 5G mobile applications. In addition, the isolation between the two antennas is better than 25 dB in the desired frequency band.

To further intuitively demonstrate the electrical performance of the proposed dual-feed antenna module, its current distribution and illustrative far-field radiation patterns are shown in Fig. 6 and Fig. 7 respectively. It can be seen from Fig. 6 that when Port 1 is excited, the antenna is working in PIFA mode as the majority of currents are concentrating in its radiating arm, while Port 2 is activated, it works as a full-wavelength loop antenna mode as there are two stable current nulls existing at the center of the main loop radiator. One also can observe in Fig. 6 that no matter which feed port is under operation, there is almost no current coupled to the other port, which shows the proposed design has great

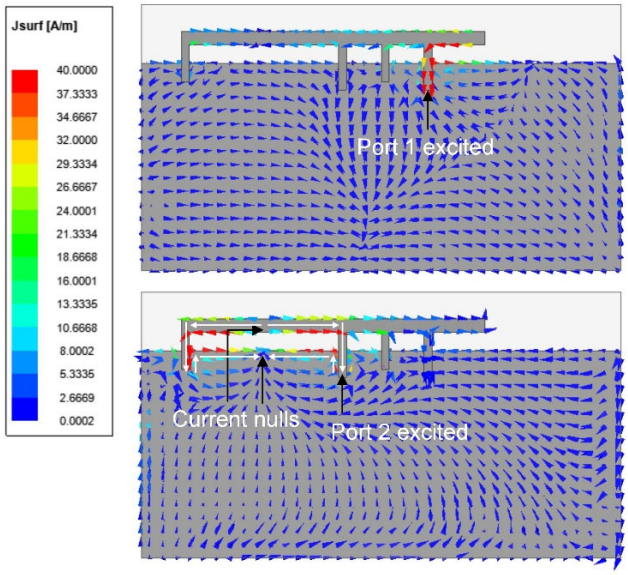

FIGURE 6. Current distribution of the dual-feed antenna module at 3.5 GHz.

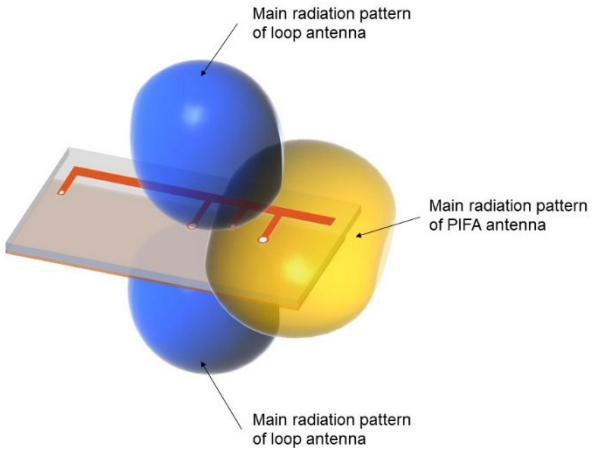

FIGURE 7. Concept map of the orthogonal radiation patterns for the dual-feed antenna module.

advantage in guaranteeing an excellent isolation between two connected antennas without any additional decoupling structures. Moreover, as depicted in Fig. 7, the far-field performance under the two ports fed separately show the radiation pattern of the loop antenna is perpendicular to the substrate while that of the PIFA antenna mainly radiates outward paralleled to the PCB. Therefore, the two types of radiation patterns are approximately orthogonal with each other, which can effectively reduce the coupling between the antennas and further verify the great isolation characteristic of the dual-feed antenna module.

B. CONSTRUCTION OF UNILATERAL QUAD-FEED MIMO ANTENNA SUBSYSTEM

A unilateral quad-feed MIMO antenna subsystem comprised of two dual-feed antenna modules with mirror-symmetrical

TABLE 2. Detail dimensions of the quad-feed MIMO antenna (unit: mm).

Parameters	Values	Parameters	Values
W_g	39	d_1	5.5
L_{sub}	130	d_2	28
W_{sub}	50	d_3	1.85
W	2.5	L_f	8.5
s	1.5	L_s	7
L	56	L_0	120.5
h	0.8	-	-

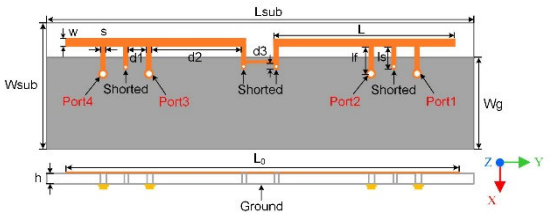

FIGURE 8. Structural diagram of the quad-feed MIMO antenna subsystem.

placement along the y-axis is presented in Fig. 8. From the side-view of the quad-feed antenna, its main radiator can be considered as a metal rim with the length of L_0, the dimension of which is close to that of a commercial 6-inch flagship mobile phone. In order to maintain the integrity of the phone rim without any breaks, a section of metal line with its both end shorted is added between the two dual-feed antenna modules and such short-circuit connection would not affect the overall MIMO antenna's performance. Note that some parameters of the quad-feed MIMO antenna subsystem are slightly different from those of the dual-feed MIMO antenna module for the purpose of obtaining a better impedance matching performance. The detail dimensions of the quad-feed antenna subsystem are listed in Table 2.

Fig. 9 shows the simulated S-parameters of the quad-feed subsystem, from which it can be seen that the isolation level among the four antennas achieves more than 17 dB within the band of 3.4∼3.6 GHz with reflection coefficient less than −10 dB. The good isolation phenomenon can also be

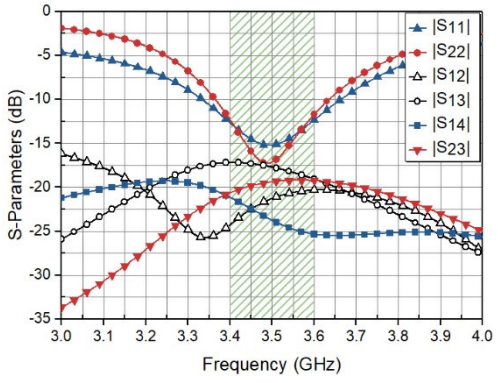

FIGURE 9. Simulated S-parameter of the quad-feed MIMO antenna subsystem.

viewed in the current distribution when one of the antenna ports is excited, as plotted in Fig. 10, where limited current distribution is found at its adjacent ports. Though compared with the dual-feed antenna module, the decoupling performance would be affected after integrating more antennas on a single metal rim, the isolation of the quad-feed antenna subsystem is still acceptable for MIMO communication of mobile terminals with such multiple antenna system.

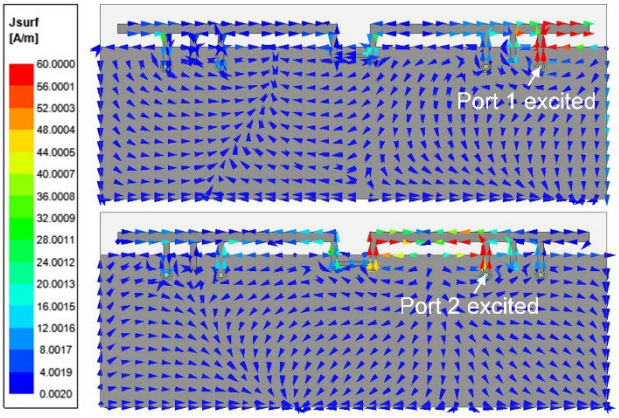

FIGURE 10. Current distribution of the quad-feed antenna subsystem at 3.5 GHz.

C. DECOUPLING OF PLANAR EIGHT-FEED MIMO ANTENNA SYSTEM

Based on the multi-feed antenna architecture proposed in the previous sections, the final geometry of the planar eight-feed MIMO antenna system is obtained and shown in Fig. 11 [23], the dimension of which is 130 mm × 70 mm.

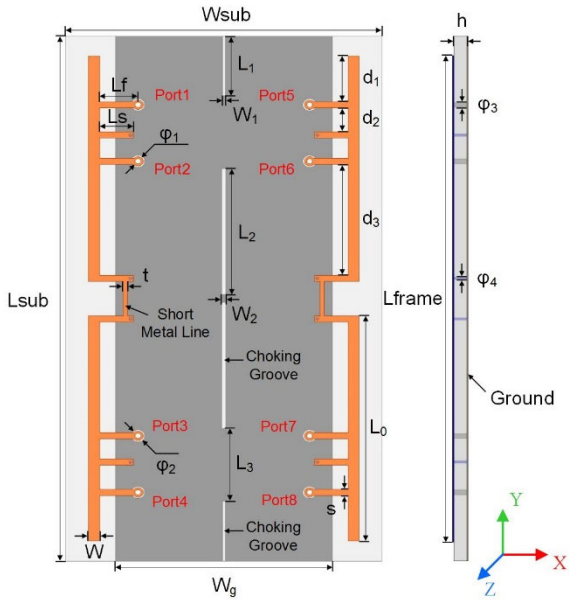

FIGURE 11. Structural diagram of the planar eight-feed MIMO antenna system.

TABLE 3. Detail dimensions of the eight-feed MIMO antenna (unit: mm).

Parameters	Values	Parameters	Values	Parameters	Values
W_g	48	φ_1	1.15	L_3	18
L_{sub}	130	φ_2	1.5	W_1	0.2
W_{sub}	70	φ_3	0.65	W_2	0.4
L_{frame}	120	φ_4	0.3	d_1	11.3
W	2.5	L_f	8.5	d_2	6
s	1.5	L_s	7.4	d_3	27.5
t	0.9	L_1	14.8	L_0	55.8
h	0.8	L_2	31.2	-	-

The detail dimensions are given in Table 3. As the eight-feed MIMO antenna system is comprised of two quad-feed MIMO antenna subsystems located on both long edge of the mobile terminal, the isolation between unilateral ports can be enhanced by fine tuning several key parameters such as d2, L_s and L_f. However, strong coupling still exists among the feed ports opposite to each other along the two metal rims on both long edge of the terminal, i.e., Port 1 and Port 5, Port 2 and Port 7. In order to reduce such mutual couplings, four choking grooves are etched along the center line of the ground plane with different lengths and widths, which can be separated into two groups, i.e., groove 1 (L_1, W_1) and groove 2 (L_2, W_2). Fig. 12 shows the parametric study of the two groups, from

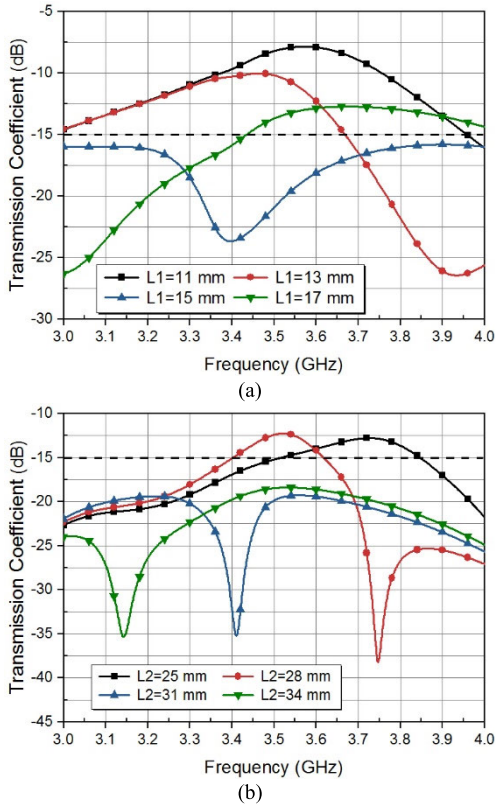

FIGURE 12. Parametric study of the chocking grooves on the effect of the multi-feed antenna isolation. (a) Simulated |S15| (isolation between Port 1 and Port 5) with different L1. (b) Simulated |S27| (isolation between Port 2 and Port 7) with different L2.

which it can be observed that the grooves' lengths of L1 and L2 have varying degrees of impact on the isolation of the opposite feed-ports. Considering isolation level of more than 15 dB as a benchmark, as well as taking their influence on the resonance frequency into account, $L_1 = 14.8$ mm and $L_2 = 31$ mm are finally selected for the proposed design after optimization using EM simulators.

In order to further demonstrate the decoupling capability of the four chocking grooves, the vector current diagram of the eight-feed MIMO antenna system when Port 1 and Port 2 are excited respectively with and without the grooves is depicted in Fig. 13. It can be seen from the current distributions that after adding the choking grooves, the coupling currents concentrate on the grooves instead of flowing to the opposite antennas so that the mutual coupling is greatly reduced. Additionally, as comparison, two counterpart eight element MIMO antenna arrays constructed in a traditional way without any additional decoupling structures are also investigated in this work. Each of the counterpart MIMO antenna array consists of eight identical PIFA antennas with different intervals of array arrangement on the PCB, as shown in Fig. 14 (a) and Fig. 14 (b). The simulated and measured S-parameters of the two counterpart MIMO antenna arrays are shown in Fig. 15, from which one could observe that, though the operating bandwidth of the two eight-feed antenna arrays can cover the band of interest in this work, their mutual coupling among the typical adjacent or opposite ports is quite serious, which is only better than 10 dB for the antenna array shown in Fig. 14(a) and 7.5 dB for the one shown in Fig. 14(b) (both of them are taken the worst case into consideration).

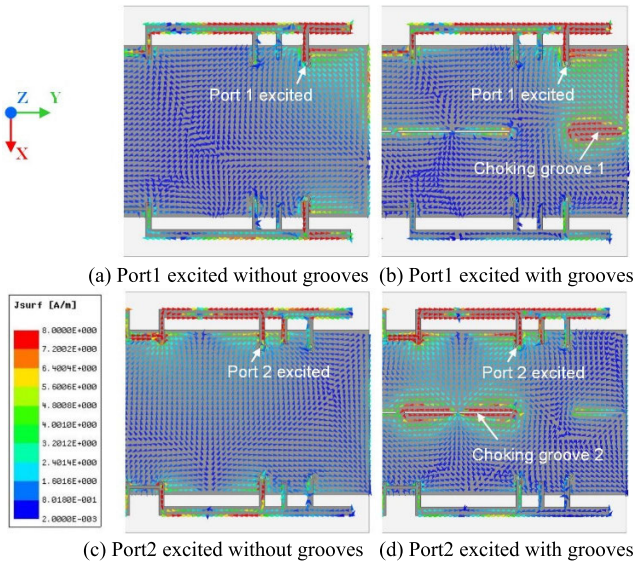

FIGURE 13. Current distributions of the planar eight-feed MIMO antenna system with and without choking grooves while Port 1 and Port 2 are excited respectively.

The final model of the proposed planar eight-feed MIMO antenna system has been fabricated and measured for performance verification, as shown in Fig. 16. The experimental

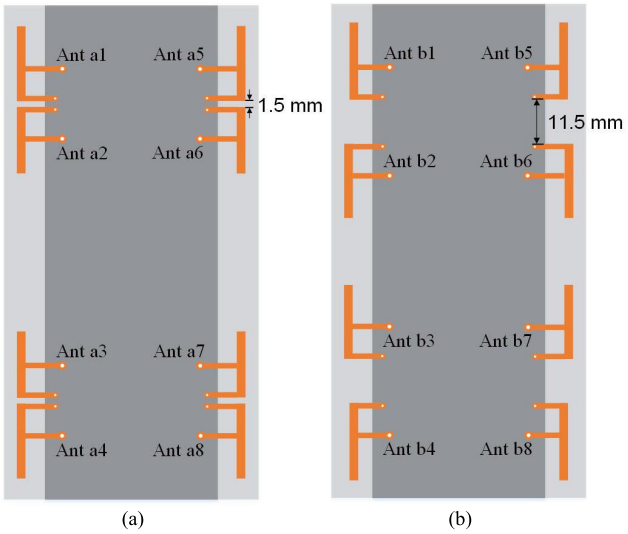

FIGURE 14. Eight-feed counterpart antenna arrays. (a) Eight compact-arranged PIFA antenna array. (b) Eight sparely-arranged PIFA antenna array.

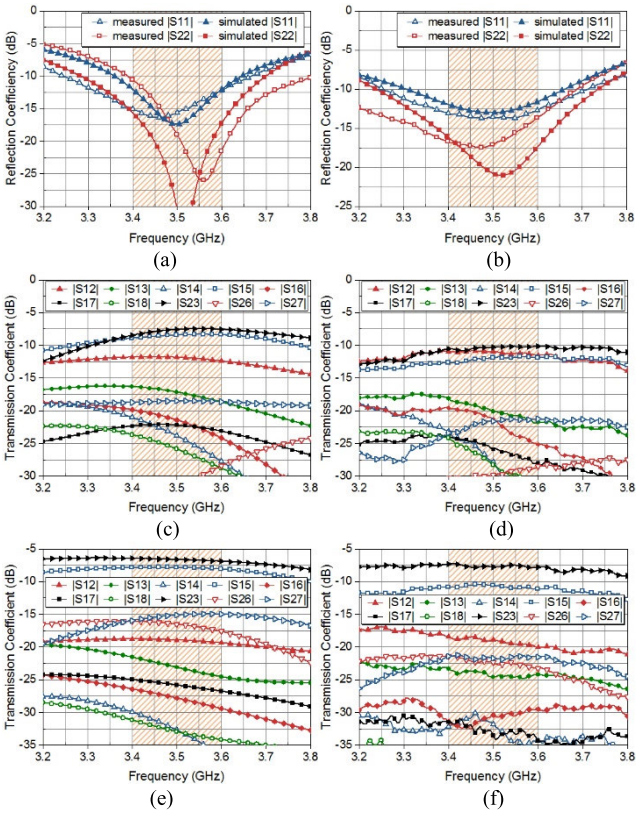

FIGURE 15. Simulated and measured S-parameter of the eight-feed MIMO counterpart antenna arrays. (a) and (b) are the simulated and measured reflection coefficients of the arrays shown in Fig. 14(a) and Fig. 14(b) respectively. (c) and (d) are the simulated and measured isolation of the array shown in Fig. 14(a) respectively. (e) and (f) are the simulated and measured isolation of the array shown in Fig. 14(b) respectively.

S-parameters of the antenna system are presented in Fig. 17 associated with simulated data for comparison. Due to the symmetrical characteristic of the whole antenna system,

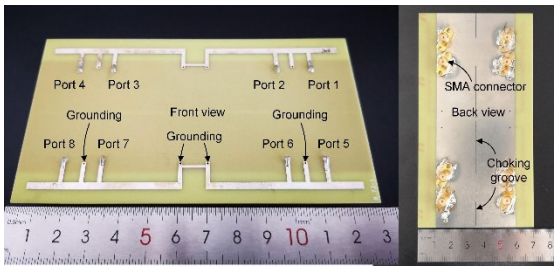

FIGURE 16. Prototype photograph of the planar eight-feed MIMO antenna system.

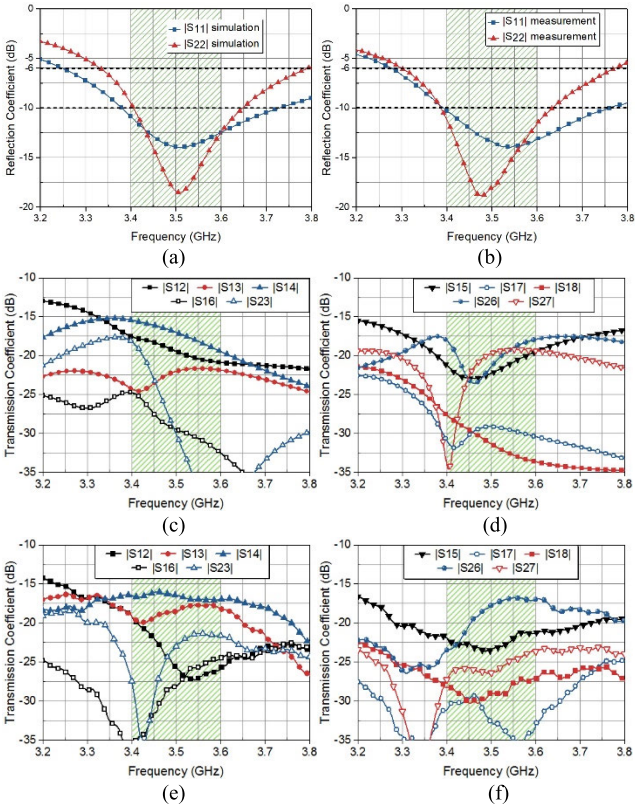

FIGURE 17. Simulated and measured S-parameter of proposed planar eight-feed MIMO antenna system. (a) and (b) are the simulated and measured reflection coefficients respectively. (c) and (d) are the simulated isolation between the selected feed-ports. (e) and (f) are the measured isolation between the selected feed-ports.

only the results of selected feed-ports are included in the figure. Though certain discrepancies are observed due to minor fabrication tolerance, both the simulated and experimental results agree with each other well. The measured operating bandwidths of the PIFA antenna excited at Port 1 and the loop antenna excited at Port 2 are 3.38∼3.75 GHz (10.4% fractional bandwidth) and 3.38∼3.63 GHz (7.1% fractional bandwidth) with reflection coefficient less than −10 dB, respectively. The isolation levels within the band of 3.4∼3.6 GHz are better than 15 dB among the different feed-ports, which verifies that the decoupling performance of the proposed design is much better than that of the traditional ones as shown in Fig. 14. Furthermore, the radiation pattern and efficiency of the proposed antenna are conducted in a

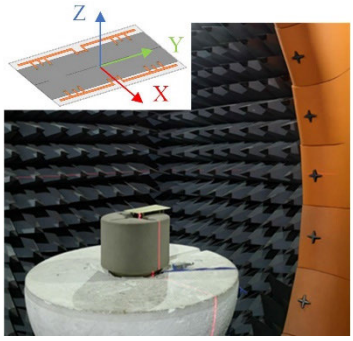

FIGURE 18. Radiation pattern measurement setup for the planar eight-feed MIMO antenna system.

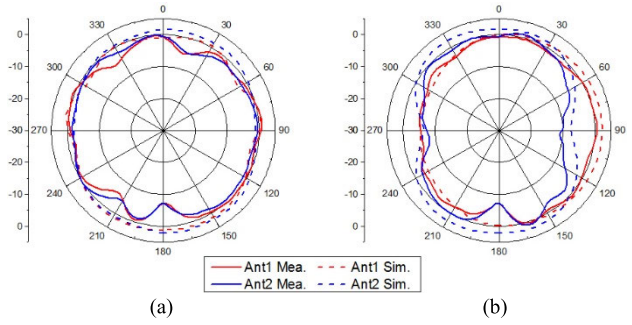

FIGURE 19. Simulated and measured 2-D radiation patterns of the planar eight-feed MIMO antenna system under Port1 and Port2 excited. (a) Radiation patterns in yoz-plane. (b) Radiation patterns in xoz-plane.

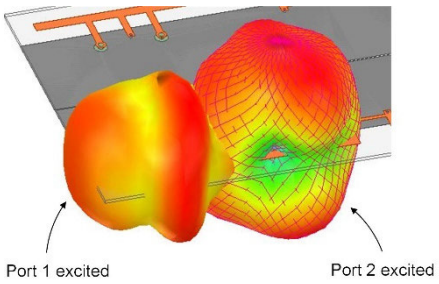

FIGURE 20. 3-D radiation pattern of the planar eight-feed MIMO antenna system under Port1 and Port2 excited in simulation at 3.5 GHz.

near-field anechoic chamber, as shown in Fig. 18. Both of the simulated and measured two-dimensional (2-D) radiation patterns are plotted in Fig. 19 and a three-dimensional (3-D) radiation pattern exported from simulation is given in Fig. 20. It can be concluded from these results that:

1) The radiation patterns of the whole eight-feed antenna system can be separated into four identical groups.
2) Within each group, there are two almost orthogonal radiation patterns generated while one of the two ports are excited, respectively.
3) Within each group, the radiation patterns are also complementary to each other, enabling quasi-omnidirectional beam coverage capability in a real complex multipath environment.

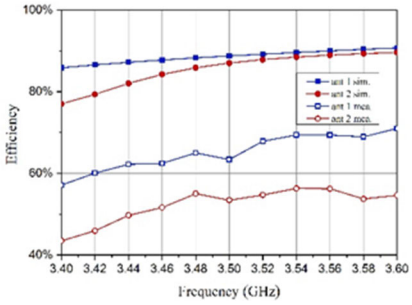

FIGURE 21. Measured efficiency of the planar eight-feed MIMO antenna system.

Besides, the experimental results of the total efficiencies against frequencies are presented in Fig. 21. The total efficiencies of the PIFA antenna excited at Port 1 and the loop antenna excited at Port 2 achieve 65% and 55% at 3.5 GHz, respectively.

D. IMPACT OF USER'S BODY

In this section, to analyze the impacts of the human body on the antenna array, the simulated 8 × 8 MIMO antenna array with one hand and two hands modes are analyzed in HFSS.

For the one hand mode, as shown in Fig. 22(a) and (c), due to the appearance of the thumb, it covered a huge area of a Loop antenna's radiation space, which caused the offset of the impedance matching of Ant2 which is acceptable in general. However, the rest of the impedance matching almost unchanged and all of the isolation of ports had different degrees of improved for 1-2dB as illustrated in Fig. 22(e) and (g). Yet, gain and total efficiency had a reasonable loss due to the high absorption loss of the user's hand as seen in Fig. 22(i).

For the two hands held mode, the antenna array is clipped into the palm of the two hands which kept the ten fingers away from radiation area, as shown in Fig. 22(b) and (d), so that it causes an extremely subtle impacts on the impedance matching and isolation of all ports as illustrated in Fig. 22(f) and (h). Yet, gain and total efficiency had a subtle loss because of the two hands' slight absorption in the near field as seen in Fig. 22(j).

To analyze the user's hand and head impacts on the proposed MIMO antenna arrays, we simulated this mode that combine with the one hand mode and a human head as seen in Fig. 23(a). As shown in Fig. 23(b)-(d), apparently, the hand had a major influence on the radiation of antenna array in this mode because of its coverage and therefore have similar performance with a hand mode above. Yet, gain and total efficiency had a great loss as illustrated in Fig. 23(e) because the head and hand compare with one hand and two hands modes.

To calculate the SAR of the antenna, we simulated 8 × 8 MIMO antenna array with one hand held near the head which selected from component libraries in CST microwave studio

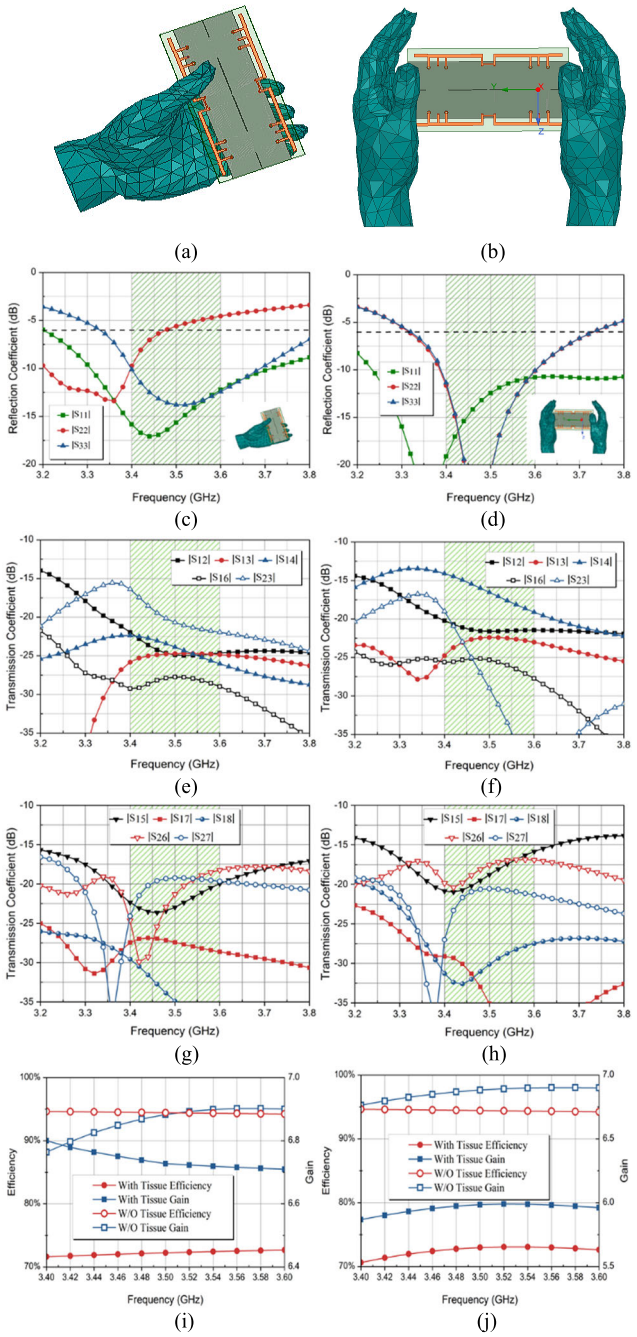

FIGURE 22. Simulated the impacts of the user's hands on antenna performance. (a) a hand mode, (c) the reflection coefficient, (e) and (g) transmission coefficient, (i) total efficiency and gain in one hand mode. (b) two hands mode, (d) the reflection coefficient, (f) and (h) transmission coefficient, (j) total efficiency and gain in two hands mode.

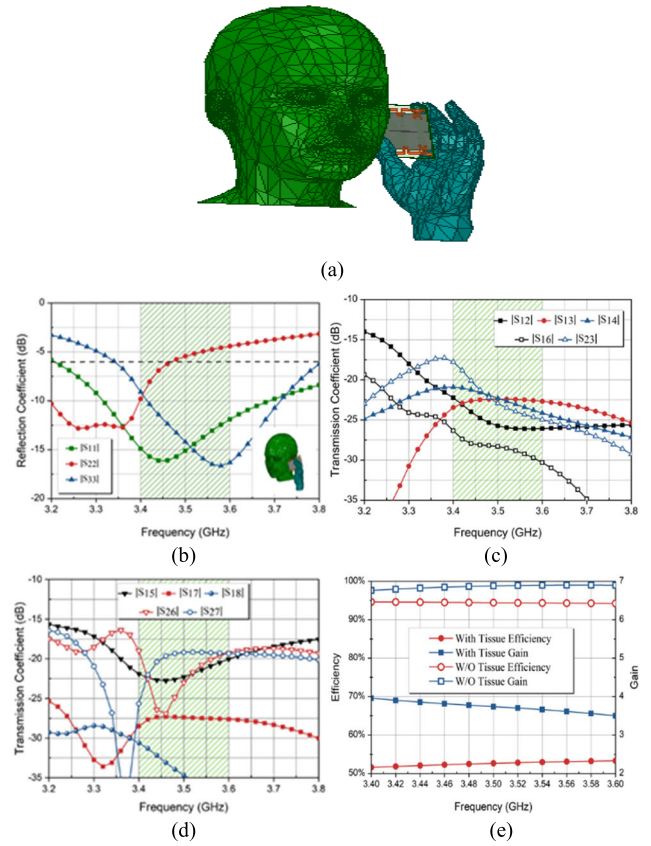

FIGURE 23. Simulated the impacts of the user's body on antenna performance. (a)-(e) the reflection coefficient, transmission coefficient, total efficiency and gain in head and hand mode.

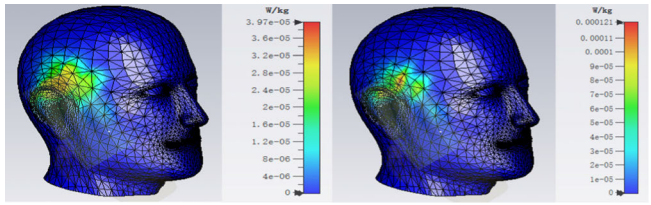

FIGURE 24. SAR of the antenna is calculated in (a) 10gm and (b) 1gm.

as shown in Fig. 24(a)-(b). We calculated SAR of the antenna in two different standards which is 10gm and 1gm of tissue.

III. EIGHT-FEED MIMO ANTENNA SYSTEM DESIGNED WITH PRACTICAL CURVED METAL-RIMS

In order to reduce the space occupation of the planar eight-feed MIMO antenna system to the mobile phone and make the proposed antenna further adapted to practical phone industry design (ID), the 2-D eight-feed antenna scheme is transformed to 3-D MIMO antenna structure and an eight-feed MIMO antenna system designed on practical curved metal-rims is proposed in this section. The top-view and front-view of the antenna configuration are sketched in Fig. 25 and Fig. 26, the size of which is similar to the commercial phone model iPhone Xs Max. The curved metal-rims are manufactured with the advantage of 3-D printing technology [24]. Fillets with radius, R, are employed at the four corners of the FR-4 substrate according to the actual phone' appearance. After applying the multi-feed technology and the proposed design methodology to realize the eight-feed MIMO antenna system on the practical phone rims, it can leave enough

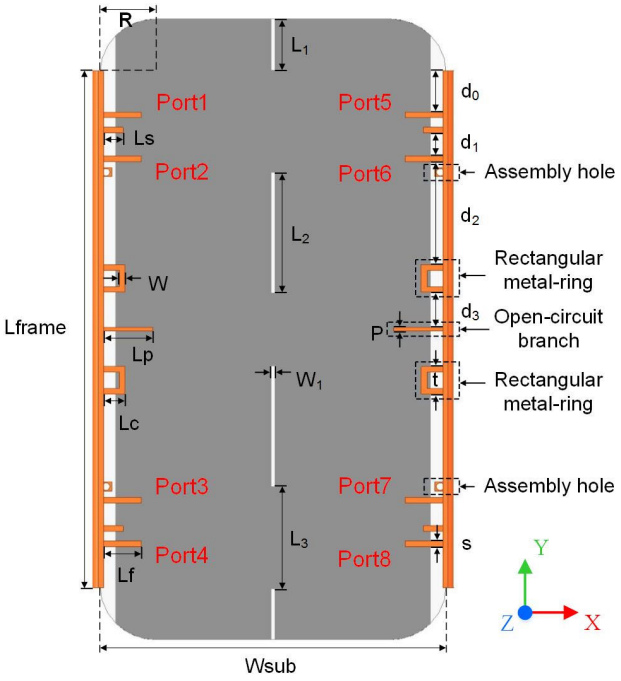

FIGURE 25. The top-view of the eight-feed MIMO antenna system with curved metal-rims.

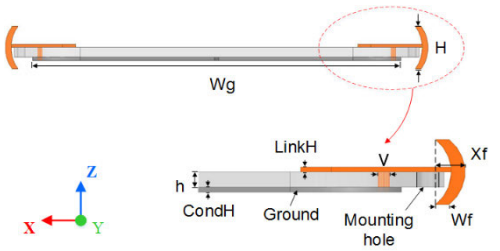

FIGURE 26. The front-view of the eight-feed MIMO antenna system with curved metal-rims.

space to the top and bottom portion of the mobile phone to accommodate other functional antennas like 3G/4G antennas and WBG (Wi-Fi Bluetooth and GPS) antennas, which makes the proposed 5G MIMO antenna system very compatible with the existing antennas.

Similar to the planar eight-feed MIMO antenna system in Fig. 11, four choking grooves are also etched on the ground plane to improve the port isolation. It is acceptable since even commercial flagship phones have almost periodic grooves on the main board for heat dissipation and weight reduction. There are four assembly holes designed on the metal-rims to ease the fixation between the rims and the substrate. Furthermore, different from the planar model, the short metal line is replaced by an open-circuit branch with size of (l_p, p) for the integrity of the whole metal rim. Meanwhile, rectangular metal-rings with size of (l_c, t, w) are added in the metal-rims in order to reduce the actual electrical length of the loop antennas. The detail dimensions of the eight-feed MIMO antenna system with curved metal-rims are given in Table 4.

TABLE 4. Detail dimensions of the curved metal-rimmed eight-feed MIMO antenna (unit: mm).

Parameters	Values	Parameters	Values	Parameters	Values
W_g	80	L_p	10	d_1	6.3
L_{frame}	140	L_c	7	d_2	28.3
W_{sub}	89	L_f	11	d_3	9.7
W	1.5	L_s	6.5	H	6.5
s	1.5	L_1	14	$LinkH$	1
t	7.5	L_2	31	V	0.6
h	0.8	L_3	30	X_f	2.8
R	14	W_1	1	W_f	1.3
P	1	d_0	11.3	-	-

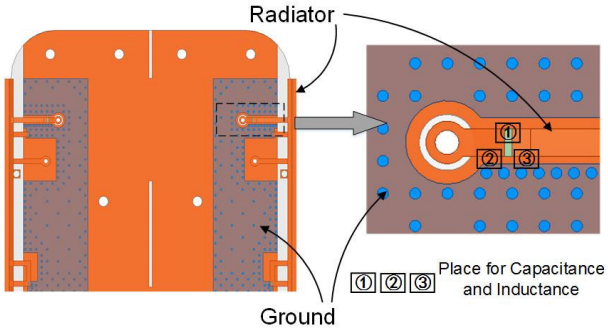

FIGURE 27. π-shaped matching network implementation.

In order to further improve the impedance matching of the complete MIMO antenna system, a π-shaped LC matching network can be inserted to the feed-ports. LC matching network is an efficient impedance tuning technique commonly used by and widely known to professional antenna engineers, which is demonstrated in Fig. 27. Therefore, according to the on-site measured results of antenna reflection coefficient, different values of inductor or capacitor can be easily introduced to improve the ports' impedance matching with the help of VNA and smith chart.

A. EXPERIMENTAL RESULTS

The final prototype of the proposed eight-feed MIMO antenna system realized in the curved metal-rims is shown in Fig. 28. The comparison between the simulated and measured S-parameters is given in Fig. 29, from which it can be observed that a good agreement is achieved and the operating bandwidth can well cover the desired frequency band of 3.4∼3.6 GHz with reflection coefficient less than −10 dB or 3.3∼3.8 GHz with reflection coefficient less than −6 dB when all port isolations are better than 15 dB.

In order to analyze the influence of the added rectangular metal-rings shown in Fig. 25 on the antenna impedance matching, parametric study on the key parameter, t, is conducted, which is directly relevant to the perimeter of the ring. As seen from the results shown in Fig. 30(a), the resonant frequencies of the loop antenna (Port 2 excited) shift to lower band when t increases, which verifies that the additional metal-rings can effectively adjust the electrical length of the

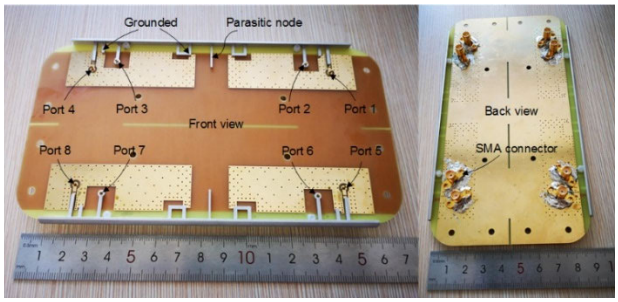

FIGURE 28. Prototype photograph of the eight-feed MIMO antenna system with curved metal-rims.

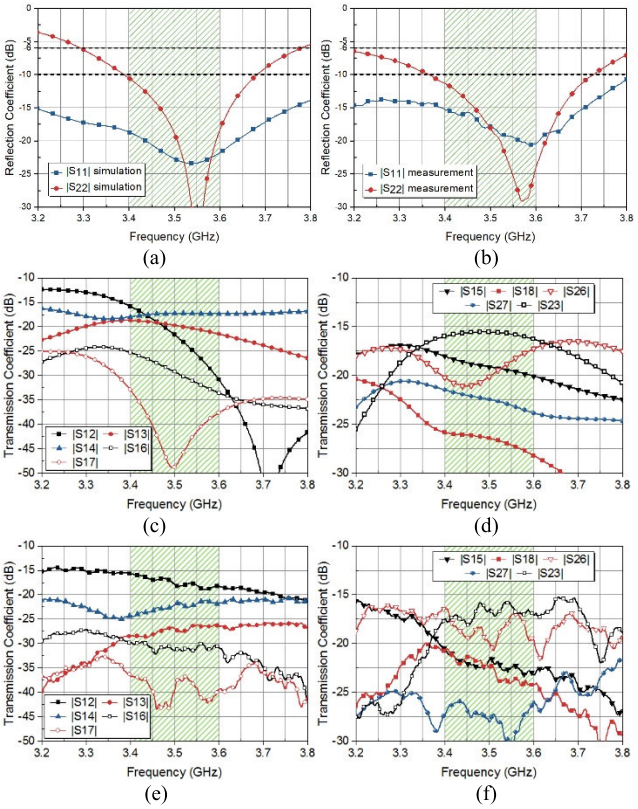

FIGURE 29. Simulated and measured S-parameter of proposed eight-feed MIMO antenna system with curved metal-rims. (a) and (b) are the simulated and measured reflection coefficients respectively. (c) and (d) are the simulated isolation between the selected feed-ports. (e) and (f) are the measured isolation between the selected feed-ports.

loop antenna. Meanwhile, Fig. 30(b) demonstrates the effect of the length of the open-circuit branch (l_p) on the antenna decoupling, where the isolation between Port 2 and Port 3 (|S23| in dB) is chosen for the analysis. As l_p increases, the coupling effect can be effectively reduced, especially when l_p is around $\lambda/8$, an optimum decoupling effect can be obtained. A further study on the decoupling effect of the open-circuit branch can be viewed in the antenna current distributions with and without the branch, as shown in Fig. 31, where the coupling energy is significantly reduced after including the open-circuit branch.

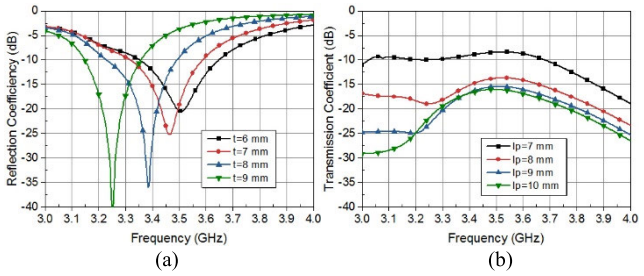

FIGURE 30. Parametric study of the rectangular metal-ring on the effect of the multi-feed antenna. (a) Simulated |S22| (Port 2 excited only) with different t. (b) Simulated |S23| with different l_p (isolation between Port 2 and Port 3).

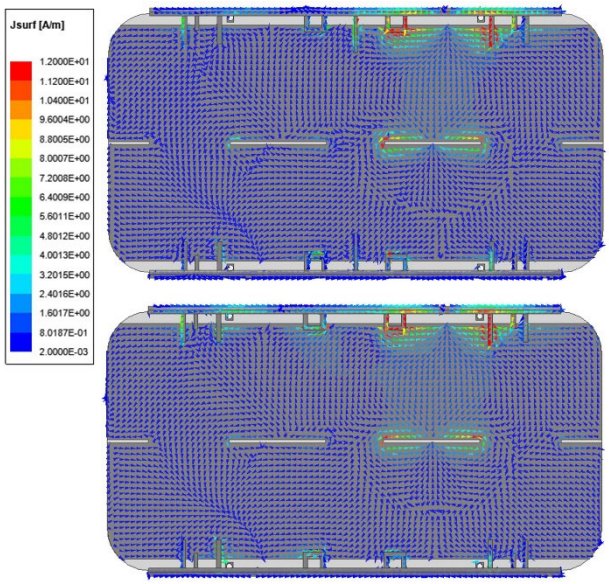

FIGURE 31. Current distributions of the curved metal-rimmed eight-feed MIMO antenna system with and without the open-circuit branch at 3.5 GHz.

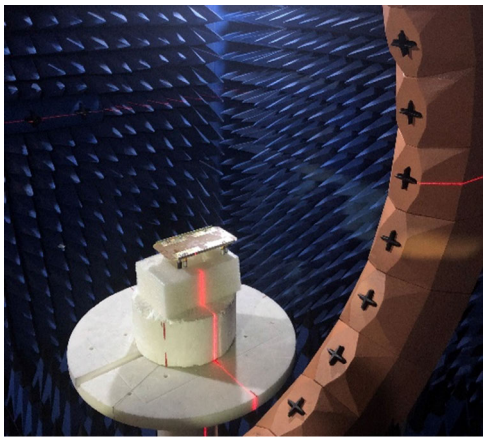

FIGURE 32. Radiation pattern measurement setup for the curved metal-rimmed eight-feed MIMO antenna system.

Radiation patterns of the eight-feed MIMO antenna system are also tested in the anechoic chamber for complete performance verification, as shown in Fig. 34. Similar to the planar

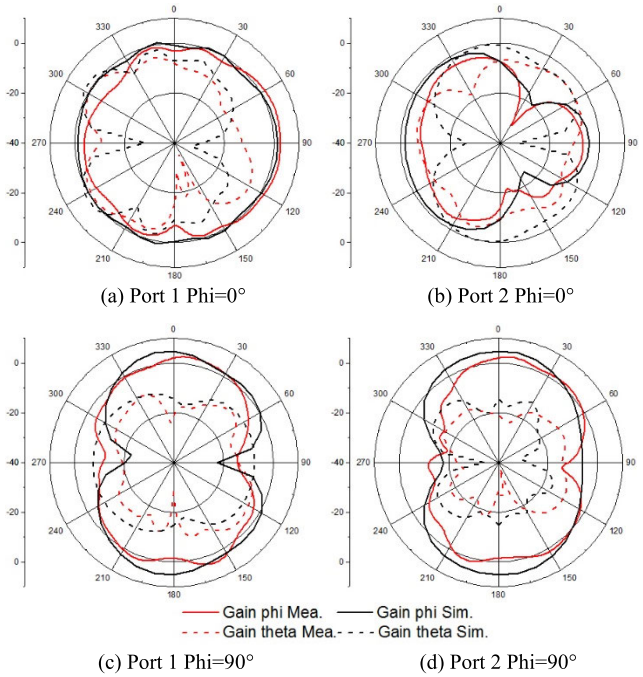

FIGURE 33. Simulated and measured 2-D radiation patterns of the curved metal-rimmed eight-feed MIMO antenna system while Ports 1 and 2 are excited respectively.

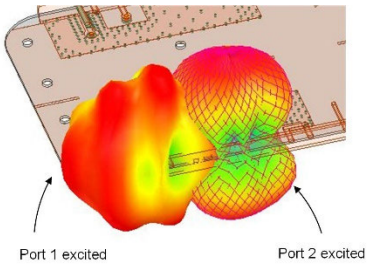

FIGURE 34. 3-D radiation patterns of the curved metal-rimmed eight-feed MIMO antenna system under Port1 and Port2 excited in simulation at 3.5 GHz.

eight-feed MIMO antenna mentioned in the last section, the proposed metal-rimmed MIMO antenna system also possesses approximately orthogonal radiation patterns between the PIFA modes and the loop modes, which can be viewed in the 2-D radiation patterns plotted in Fig. 33 and the 3-D simulated radiation patterns plotted in Fig. 34. Such radiation patterns diversity is beneficial to the isolation enhancement and good for mobile wireless communication with reduced cross-talk.

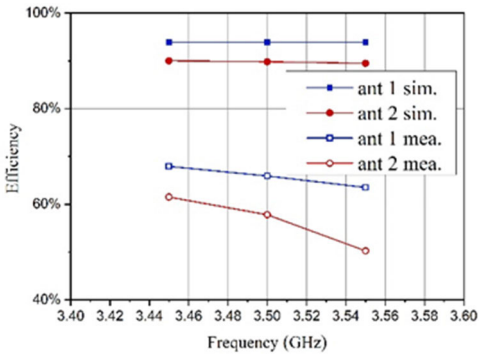

FIGURE 35. Measured radiation efficiencies of the curved metal-rimmed eight-feed MIMO antenna system under Port1 and Port2 excited.

The measured efficiencies of the eight-feed MIMO antenna system with curved metal-rims are given in Fig. 35. High total efficiencies of 66% and 57% at 3.5 GHz can be achieved when Port 1 and Port 2 are functioned respectively.

Moreover, ECC is another key indicator to evaluate the data transmission rate for 5G application. After obtaining the field data from the measured radiation patterns, the ECC can be calculated through (2), as shown at the bottom of the page, where XPD is the cross-polarization discrimination; $p_\theta(\Omega)$ and $p_\phi(\Omega)$ are angular distribution of the θ and ϕ component.

In the context of mobile terminals, uniform angular distribution and equal polarization (XPD = 1) is always assumed, therefore, equation (2) can be further simplified to be:

$$\rho_e = \frac{\left|\iint_{4\pi}\left[\vec{E}_1(\theta,\varphi)\cdot\vec{E}_2(\theta,\varphi)\right]d\Omega\right|^2}{\iint_{4\pi}\left|\vec{E}_1(\theta,\varphi)\right|^2 d\Omega \iint_{4\pi}\left|\vec{E}_2(\theta,\varphi)\right|^2 d\Omega} \tag{3}$$

where

$$\vec{E}_1(\theta,\varphi)\cdot\vec{E}_2(\theta,\varphi) = E_{\theta 1}(\theta,\varphi)\cdot E^*_{\theta 2}(\theta,\varphi) + E_{\phi 1}(\theta,\varphi)\cdot E^*_{\phi 2}(\theta,\varphi) \tag{4}$$

Among the eight antennas shown in Fig. 36, the results of the calculated ECC from measure radiated fields shown in Fig. 37 reveal that the overall ECCs are lower than 0.3 in the band of interest, which satisfies the required ECCs < 0.5 for the MIMO system and validates the correlation level of the proposed MIMO antenna system is very low [25].

$$\rho_e = \frac{\left|\iint_{4\pi}\left(XPD\cdot E_{\theta 1}(\Omega)\cdot E^*_{\theta 2}(\Omega)\cdot p_\theta(\Omega) + E_{\phi 1}(\Omega)\cdot E^*_{\phi 2}(\Omega)\cdot p_\phi(\Omega)\right)d\Omega\right|^2}{\iint_{4\pi}\left(XPD\cdot G_{\theta 1}(\Omega)\cdot p_\theta(\Omega) + G_{\phi 1}(\Omega)\cdot p_\phi(\Omega)\right)d\Omega \cdot \iint_{4\pi}\left(XPD\cdot G_{\theta 2}(\Omega)\cdot p_\theta(\Omega) + G_{\phi 2}(\Omega)\cdot p_\phi(\Omega)\right)d\Omega} \tag{2}$$

TABLE 5. Comparison between the proposed antenna and the reported antennas.

Ref.	[27]	[28]	[29]	[30]	Proposed
Metal rim	Metal	Metal & Dielectric board	Metal & Dielectric board	Metal	Metal
Frame slot/breaks for MIMO	4	4	0	8	0
LC matching	yes	yes	yes	Yes*	yes
BW (-6 dB)	3.4-3.6 GHz	3.4-3.6 GHz	3.4-3.6 GHz	3.3-5 GHz	3.3-3.8 GHz
BW (-10 dB)	3.475-3.6 GHz	3.44-3.59 GHz	Narrower than 3.4-3.6 GHz	3.5-4.85 GHz (monopole) 4.5-5 GHz (dipole)	3.4-3.7 GHz
Orthogonal antenna unit $\|S_{ij}\|$ (dB)	>19	>20.1	>24.2	>21	>25
Array worst $\|S_{ij}\|$ (dB)	>16	>12.7	>15.7	>12	>15
ECC	<0.05	<0.13	N/A	<0.11	<0.3
Eff. (%)	59-73	35.2-64.7	>38	31.6-74.7	50-68
MIMO	8×8	8×8	8×8	8×8	8×8

Ref.: reference; BW: bandwidth; Eff.: efficiency; *: besides LC matching, balun chips are needed; N/A: not available in original paper.

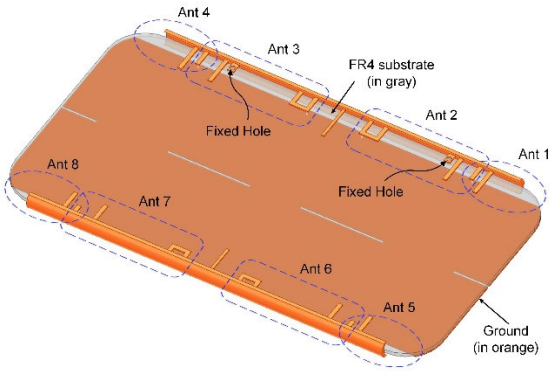

FIGURE 36. Schematic diagram of the curved metal-rimmed eight-feed MIMO antenna system marked with four PIFA antennas (Ant 1, Ant 4, Ant 5, and Ant 8) and four dual-loop antennas (Ant 2, Ant 3, Ant 6, and Ant 7).

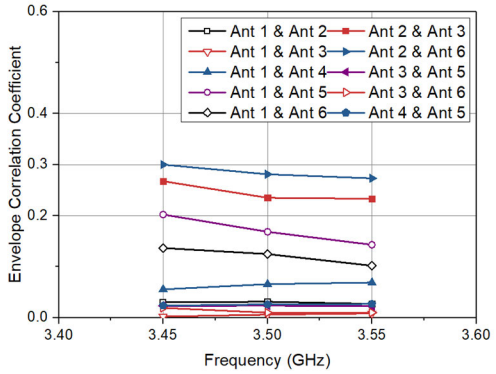

FIGURE 37. ECC results of the curved metal-rimmed eight-feed MIMO antenna system.

B. PERFORMANCE COMPARISON WITH REPORTED DESIGNS

In order to highlight the advantages of the proposed multi-feed MIMO antenna with curved metal-rims, Table 5 summarizes the performance comparison between this work and the reported designs in literatures [27]–[30]. One can observe from the table that the proposed antenna system has simpler structure of realizing an eight-feed MIMO antenna system by directly exciting the metal frame, which does not occupy extra space of the smartphone and possesses an excellent compatibility with existing antennas. Therefore, the proposed design is a promising antenna candidate for the application to various terminal devices with enhancing the metal rims' integrity and robustness.

IV. CONCLUSION

In this paper, an eight-port metal-rimmed MIMO antenna system using multi-feed technology is proposed for 5G mobile phone applications. The MIMO antenna system is simply constructed on the side metal-rims without breaks, but meanwhile realizes satisfactory isolation levels among the antennas without introducing additional decoupling structures. The proposed work starts with the investigation of a dual-feed antenna module, the operating principle of which has been analyzed in detail based on the multi-feed technology. Subsequently, a quad-feed and eight-feed MIMO antennas with planar structure are designed and their performance has been confirmed with experimental results. In order to adapt the proposed design to a more practical mobile phone, an eight-feed MIMO antenna system realized in curved metal-rims is finally constructed and investigated. Experimental results show that the isolation levels among the eight feed-ports are more than 15 dB from 3.4GHz to 3.6 GHz with reflection coefficient less than −10 dB and the isolation levels among the eight feed-ports are more than 15 dB from 3.3GHz to 3.8 GHz with reflection coefficient less than −6 dB. The radiation efficiency and ECC reach to at least 57% and less than 0.3 at the center frequency respectively. Such satisfactory performance validates the proposed multi-feed MIMO antenna design is particularly suitable for mobile terminal

devices which require the metal-rims to function as MIMO antennas but maintain the structural integrity and robustness.

REFERENCES

[1] WRC-15 Press Release. *World Radio Communication Conference Allocates Spectrum for Future Innovation*. Accessed: Nov. 27, 2015. [Online]. Available: http://www.itu.int/net/pressoffice/press_releases/2015/56.aspx
[2] M. A. Jensen and J. W. Wallace, "A review of antennas and propagation for MIMO wireless communications," *IEEE Trans. Antennas Propag.*, vol. 52, no. 11, pp. 2810–2824, Nov. 2004.
[3] T. Svantesson, "Correlation and channel capacity of MIMO systems employing multimode antennas," *IEEE Trans. Veh. Technol.*, vol. 51, no. 6, pp. 1304–1312, Nov. 2002.
[4] J. Y. Deng, J. Li, L. Zhao, and L. Guo, "A dual-band inverted-F MIMO antenna with enhanced isolation for WLAN applications," *IEEE Antennas Wireless Propag. Lett.*, vol. 16, pp. 2270–2273, 2017.
[5] S. Zhang, B. K. Lau, Y. Tan, Z. Ying, and S. He, "Mutual coupling reduction of two PIFAs with a T-shape slot impedance transformer for MIMO mobile terminals," *IEEE Trans. Antennas Propag.*, vol. 60, no. 3, pp. 1521–1531, Mar. 2012.
[6] S. Zhang, S. Khan, and S. He, "Reducing mutual coupling for an extremely closely-packed tunable dual-element PIFA array through a resonant slot antenna formed in-between," *IEEE Trans. Antennas Propag.*, vol. 58, no. 8, pp. 2771–2776, Aug. 2010.
[7] J.-Y. Lee, S.-H. Kim, and J.-H. Jang, "Reduction of mutual coupling in planar multiple antenna by using 1-D EBG and SRR structures," *IEEE Trans. Antennas Propag.*, vol. 63, no. 9, pp. 4194–4198, Sep. 2015.
[8] J. L. Guo, L. Cui, C. Li, and B. H. Sun, "Side-edge frame printed eight-port dual-band antenna array for 5G smartphone applications," *IEEE Trans. Antennas Propag.*, vol. 66, no. 12, pp. 7412–7417, Dec. 2018.
[9] K.-L. Wong, J.-Y. Lu, L.-Y. Chen, W.-Y. Li, and Y.-L. Ban, "8-antenna and 16-antenna arrays using the quad-antenna linear array as a building block for the 3.5-GHz LTE MIMO operation in the smartphone," *Microw. Opt. Technol. Lett.*, vol. 58, no. 1, pp. 174–181, Jan. 2016.
[10] K.-L. Wong, J.-Y. Lu, L.-Y. Chen, W.-Y. Li, Y.-L. Ban, and C. Li, "16-antenna array in the smartphone for the 3.5-GHz MIMO operation," in *Proc. Asia–Pacific Microw. Conf. (APMC)*, Nanjing, China, Dec. 2015, pp. 1–3.
[11] L. Zhao and K.-L. Wu, "A dual-band coupled resonator decoupling network for two coupled antennas," *IEEE Trans. Antennas Propag.*, vol. 63, no. 7, pp. 2843–2850, Jul. 2015.
[12] K. Qian, L. Zhao, and K.-L. Wu, "An LTCC coupled resonator decoupling network for two antennas," *IEEE Trans. Microw. Theory Techn.*, vol. 63, no. 10, pp. 3199–3207, Oct. 2015.
[13] L. Zhao, F. Liu, X. Shen, G. Jing, Y.-M. Cai, and Y. Li, "A high-pass antenna interference cancellation chip for mutual coupling reduction of antennas in contiguous frequency bands," *IEEE Access*, vol. 6, pp. 38097–38105, 2018.
[14] L. Qu, H. Lee, H. Shin, M.-G. Kim, and H. Kim, "MIMO antennas using controlled orthogonal characteristic modes by metal rims," *IET Microw., Antennas Propag.*, vol. 11, no. 7, pp. 1009–1015, Feb. 2017.
[15] X. Zhao, S. P. Yeo, and L. C. Ong, "Decoupling of inverted-F antennas with high-order modes of ground plane for 5G mobile MIMO platform," *IEEE Trans. Antennas Propag.*, vol. 66, no. 9, pp. 4485–4495, Jun. 2018.
[16] S. Zhang, B. K. Lau, A. Sunesson, and S. He, "Closely-packed UWB MIMO/diversity antenna with different patterns and polarizations for USB dongle applications," *IEEE Trans. Antennas Propag.*, vol. 60, no. 9, pp. 4372–4380, Sep. 2012.
[17] M.-Y. Li, Y.-L. Ban, and Z.-Q. Xu, "Eight-port orthogonally dual-polarized antenna array for 5G smartphone applications," *IEEE Trans. Antennas Propag.*, vol. 64, no. 9, pp. 3820–3830, Sep. 2016.
[18] M.-Y. Li, Y.-L. Ban, Z.-Q. Xu, J. Guo, and Z.-F. Yu, "Tri-polarized 12-antenna MIMO array for future 5G smartphone applications," *IEEE Access*, vol. 6, pp. 6160–6170, 2017.
[19] C. F. Ding, X. Y. Zhang, C.-D. Xue, and C.-Y.-D. Sim, "Novel pattern-diversity-based decoupling method and its application to multielement MIMO antenna," *IEEE Trans. Antennas Propag.*, vol. 66, no. 10, pp. 4976–4985, Oct. 2018.
[20] P. Hallbjorner, "Dual feed monopole antenna," *IEE Proc.-Microw., Antennas Propag.*, vol. 150, no. 3, pp. 159–163, Jun. 2003.
[21] L. Liu, L. Zhao, Y. Cai, and Y. Yin, "Dual-feed MIMO antennas with one shared radiator for future 5G MIMO systems," in *Proc. 6th Asia–Pacific Conf. Antennas Propag. (APCAP)*, Xi'an, China, Oct. 2017, pp. 1–3.
[22] A. Chen, J. Zhang, L. Zhao, and Y. Yin, "A dual-feed MIMO antenna pair with one shared radiator and two isolated ports for fifth generation mobile communication band," *Int. J. RF Microw. Comput.-Aided Eng.*, vol. 27, no. 9, Nov. 2017, Art. no. e21146.
[23] G. Jing, Y. Liu, X. Zhao, and L. Zhao, "Coupling reduction of antenna array in 5G MIMO frequency band below 6GHz based on multi-feed technology," in *Proc. IEEE 2nd Int. Conf. Electron. Inf. Commun. Technol. (ICEICT)*, Harbin, China, Jan. 2019, pp. 710–712.
[24] G.-L. Huang, J.-J. Liang, L. Zhao, D. He, and C.-Y.-D. Sim, "Package-in-Dielectric liquid patch antenna based on liquid metal alloy," *IEEE Antennas Wireless Propag. Lett.*, vol. 18, no. 11, pp. 2360–2364, Nov. 2019.
[25] R. G. Vaughan and J. B. Andersen, "Antenna diversity in mobile communications," *IEEE Trans. Veh. Technol.*, vol. VT-36, no. 4, pp. 149–172, Nov. 1987.
[26] K.-L. Wong, C.-Y. Tsai, and J.-Y. Lu, "Two asymmetrically mirrored gap-coupled loop antennas as a compact building block for eight-antenna MIMO array in the future smartphone," *IEEE Trans. Antennas Propag.*, vol. 65, no. 4, pp. 1765–1778, Apr. 2017.
[27] A. Ren, Y. Liu, and C.-Y.-D. Sim, "A compact building block with two shared-aperture antennas for eight-antenna MIMO array in metal-rimmed smartphone," *IEEE Trans. Antennas Propag.*, vol. 67, no. 10, pp. 6430–6438, Oct. 2019.
[28] L. Chang, Y. Yu, K. Wei, and H. Wang, "Polarization-orthogonal co-frequency dual antenna pair suitable for 5G MIMO smartphone with metallic bezels," *IEEE Trans. Antennas Propag.*, vol. 67, no. 8, pp. 5212–5220, Aug. 2019.
[29] H. Xu, S. Gao, H. Zhou, H. Wang, and Y. Cheng, "A highly integrated MIMO antenna unit: Differential/common mode design," *IEEE Trans. Antennas Propag.*, vol. 67, no. 11, pp. 6724–6734, Nov. 2019.
[30] L. Sun, Y. Li, Z. Zhang, and Z. Feng, "Wideband 5G MIMO antenna with integrated orthogonal-mode dual-antenna pairs for metal-rimmed smartphones," *IEEE Trans. Antennas Propag.*, vol. 68, no. 4, pp. 2494–2503, Apr. 2020.
[31] Y. He, S. Lv, L. Zhao, G.-L. Huang, X. Chen, and W. Lin, "A compact dual-band and dual-polarized millimeter-wave beam scanning antenna array for 5G mobile terminals," *IEEE Access*, vol. 9, pp. 109042–109052, 2021.